Semenogelin-1 Inhibition of Mouse Sperm Hyperactivation Reveals Two Functional Domains Modulating CatSper Channel

Noemia A. P. Mariani[1], Natália C. M. Santos[1], Juliana J. Andrade[1], Alexandre D. Andrade[1], Beatriz Rezende[1], Tomás J. Steeman[2], Analia G. Novero[2], José C. de Lima Junior[3], Giulia Calderaro[1], Ana Clara F. Themer[1], Hélio Kushima[1], Mariano G. Buffone[4], Darío Krapf[2], Polina Lishko[3], Erick J. R. Silva[1].

[1]Department of Biophysics and Pharmacology, Biosciences Institute of Botucatu, São Paulo State University, Botucatu, SP, Brazil; [2]Institute of Molecular and Cellular Biology of Rosario, Rosario, SF, Argentina; [3]Department of Cell Biology and Physiology, Washington University in St. Louis, School of Medicine, St. Louis, MO, United States; [4]Institute of Biology and Experimental Medicine, Buenos Aires, BA, Argentina.

* To whom correspondence should be addressed: E-mail: ejr.silva@unesp.br; Phone: +55 14 3880-0223.

Running title: SEMG1 inhibition of sperm hyperactivation.

Keywords: Sperm motility, EPPIN, Spermatozoon, Ion Channels, Seminal Plasma, Semenogelins.

Abstract

Seminal plasma proteins play key roles in maintaining the survival and functional integrity of spermatozoa after ejaculation. Semenogelin-1 (SEMG1) is the predominant protein in the seminal plasma and a major structural component of the semen coagulum in humans and mice. SEMG1 binds EPPIN (Epididymal protease inhibitor) on the sperm surface, transiently inhibiting the acquisition of sperm motility and hyperactivation after ejaculation. Nevertheless, the molecular mechanisms underlying SEMG1-mediated inhibition of sperm hyperactivation remain unclear. We hypothesize that the SEMG1 effects are associated with the inhibition of CatSper, a sperm-specific calcium channel crucial for triggering hyperactivation. We observed that recombinant mouse SEMG1 (mSEMG1) inhibited both progressive motility and hyperactivation in a concentration-dependent manner. Notably, hyperactivation was not recovered upon NH_4Cl-induced alkalinization, suggesting that the effects of mSEMG1 are downstream of capacitation-associated intracellular alkalinization. Electrophysiological recordings revealed that mSEMG1 impaired CatSper currents at concentrations near its IC_{50} for inhibiting sperm hyperactivation. Recombinant mSEMG1 truncations mSEMG1$^{Q32-V118}$ and mSEMG1$^{R98-G375}$, but not mSEMG1$^{Y221-G375}$, independently inhibited sperm hyperactivation and CatSper currents similar to full-length mSEMG1. However, only mSEMG1$^{R98-G375}$ displayed similar EPPIN-binding capacity comparable to full-length mSEMG1, whereas mSEMG1$^{Q32-V118}$ and mSEMG1$^{Y221-G375}$ showed only minor binding. Our findings reveal that mouse SEMG1 comprises two distinct functional domains within the Q32-V118 and R98-S220 sequences, which contribute to the inhibition of sperm hyperactivation by targeting the CatSper channel, both independently and dependent on EPPIN binding. These functional domains represent promising prototypes for the design of spermiostatic molecules, offering additional avenues for non-hormonal male contraception targeting spermatozoa.

Introduction

To successfully fertilize the egg, spermatozoa must undergo their final maturation, a process named capacitation, within the female reproductive tract (1–3). Sperm capacitation entails a complex cascade of molecular and functional modifications, including cholesterol efflux from the plasma membrane, phosphorylation of sperm proteins, an increase in intracellular pH (pH_i), a rise in intracellular Ca^{2+} concentrations ($[Ca^{2+}]_i$), membrane hyperpolarization, and a shift from progressive motility to a whip-like flagellar motion known as hyperactivation (1, 4–8). Hyperactivation enables spermatozoa to detach from the oviductal epithelium, traverse the gelatinous cumulus matrix, and the fibrous zona pellucida, ultimately allowing fertilization to occur (9–12).

Among the molecular pathways involved in sperm hyperactivation, the rise in intracellular Ca^{2+} levels is the most critical (13). Even though multiple mechanisms promote Ca^{2+} influx in spermatozoa, the activation of the voltage-dependent and alkalinization-activated Ca^{2+} channel CatSper is considered the most relevant (14). The CatSper channel consists of a complex with at least ten associated proteins: four pore-forming subunits (CatSper1–4) and six accessory subunits (CatSper β, γ, δ, ε, ζ, and EFCAB9) (14, 15). This large multiprotein complex, known as CatSpermasome, is arranged as four longitudinal lines spanning the entire length of the sperm principal piece (4, 16–18), facilitating structural and functional coupling between CatSper complexes and triggering powerful Ca^{2+} waves along the sperm flagellum (19). Notably, CatSper deficiency in men and rodents leads to infertility due to a failure of sperm hyperactivation, while no other phenotypical abnormalities are observed (4, 14, 20–23).

While sperm hyperactivation is crucial for fertilization, it must remain tightly regulated until spermatozoa reach the oviduct (24). In this context, seminal plasma components play critical roles in modulating sperm hyperactivation and other capacitation-associated events (25). Semenogelin-1 (SEMG1), the predominant protein in seminal plasma, is secreted by the seminal vesicles and incorporated onto the sperm surface upon ejaculation through its interaction with EPPIN in both humans and mice (26–29). In the normal physiological scenario, SEMG1 binds to freshly ejaculated spermatozoa, acting as a decapacitation factor and blocking sperm motility, hyperactivation, and acrosome reaction (30–36). In humans, this inhibitory effect is maintained until the serine protease prostate-specific antigen (PSA) cleaves SEMG1, resulting in semen liquefaction and activation of sperm motility (37). Furthermore, SEMG1 promotes sperm survival in the uterus, as evidenced by the low viability of spermatozoa from *Semg1*$^{-/-}$ mice collected from the female reproductive tract during natural mating, causing a severe subfertility phenotype (38). Together, these findings indicate that SEMG1 has a dual role of protecting and modulating sperm function and metabolism during their journey through the female reproductive tract. However, the precise molecular mechanisms underlying SEMG1's roles and the contribution of EPPIN binding to these effects remain poorly understood.

Initial studies have indicated that the inhibitory effects of SEMG1 on sperm motility and hyperactivation are due to alterations in both pH_i and $[Ca^{2+}]_i$ (39). Building upon these findings, we hypothesize that SEMG1 inhibits CatSper activity, thereby affecting Ca^{2+} homeostasis and downstream pathways required for sperm hyperactivation. To test this hypothesis, we investigated the effects of mouse SEMG1 (mSEMG1) on sperm motility, hyperactivation, and CatSper activity. We further characterized the functional domains of SEMG1 and the relevance of EPPIN binding in mediating its effects. Our results revealed that mSEMG1 inhibits hyperactivation by modulating CatSper currents, an effect mediated by two independent domains within the Q32-V118 and R98-S220 sequences. Notably, only the R98-S220 sequence bound EPPIN, indicating that SEMG1 controls sperm hyperactivation by multiple mechanisms, both dependent and independent of EPPIN binding. Our results highlight the essential role of SEMG1 in preventing premature sperm hyperactivation and offer promising avenues for exploring its functional domains as prototypes for the rational design of ligands with male contraceptive applications targeting spermatozoa.

Results

Mouse SEMG1 inhibits sperm progressive and hyperactivated motilities

A sperm's motility pattern changes from progressive to hyperactivated during capacitation in the female reproductive tract (11, 40). Previous studies have shown that both human and mouse SEMG1 can regulate sperm function, including motility (30, 33, 41). To gain insights into the effects of SEMG1 on sperm swimming behavior, we incubated spermatozoa isolated from the cauda epididymidis in capacitating medium, which sustains hyperactivation, in the absence (control) or presence of increasing concentrations of full-length recombinant mouse SEMG1 (mSEMG1; Q32-G375). mSEMG1 did not affect the percentage of motile spermatozoa at concentrations up to 10 μM compared to control, exhibiting a moderate effect at 25 μM (~25% inhibition) after 20 min ($p=0.0005$) and 120 min ($p=0.011$) of incubation (Fig. 1A, Fig. S1, Video S1). Concurrently, mSEMG1 increased the percentage of slow spermatozoa at 10 μM ($p=0.026$) and 25 μM ($p=0.001$) after 20 min of incubation (Fig. 1B, Fig. S1). The percentage of slow spermatozoa returned to control levels after 120 min of incubation (Figure 1B, C). mSEMG1 did not affect sperm viability at the concentrations tested, confirming that its effects on sperm motility were not associated with sperm death (Fig. 1D).

On the other hand, mSEMG1 displayed a more potent effect on hyperactivated motility. mSEMG1 inhibited hyperactivated motility in a concentration-dependent manner with a calculated IC_{50} (95% confidence interval) of 5.2 μM (1.3–21.2 μM), reaching a maximum inhibition of ~90% at 25 μM ($p = 0.0003$) compared to control after 120 min (Fig. 2A, B). Consistently, 25 μM mSEMG1 decreased curvilinear velocity (VCL, $p = 0.006$) and amplitude of lateral head displacement (ALH, $p = 0.005$), kinematic parameters associated with vigorous sperm movements (Cancel et al., 2000) (Fig. 2C). Notably, these effects were not rescued by intracellular alkalization induced by NH_4Cl, a condition known to evoke sperm hyperactivation via activation of the sperm-specific Ca^{2+} channel

CatSper (42, 43) (Fig. 2D). Similarly, mSEMG1 inhibited progressive motility (IC_{50} 10.1 μM, 95% CI 2.6–38.5 μM), and decreased both average path velocity (VAP) and straight-line velocity (VSL), kinematic parameters associated with sperm progressiveness (Fig. S2). Altogether, these results indicate that mSEMG1 inhibits mouse sperm progressive motility and hyperactivation by modulating signaling pathways downstream of intracellular alkalinization.

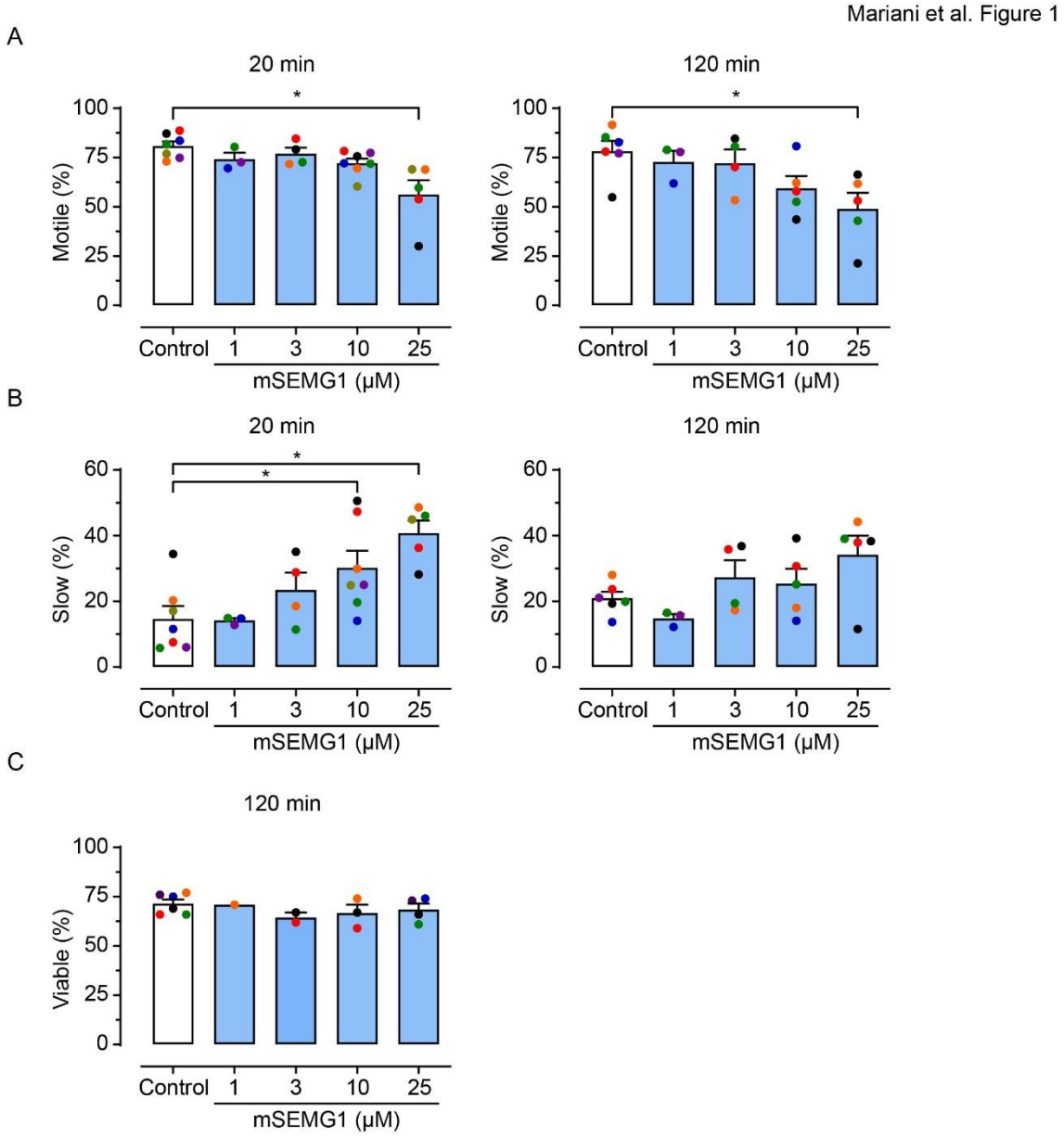

Figure 1. Effects of recombinant mouse semenogelin-1 (mSEMG1) on sperm motility and viability. A-B, Percentage of total (A) and slow (B) motility of spermatozoa after incubation with mSEMG1. **C**, Percentage of viable spermatozoa after incubation with mSEMG1. Spermatozoa were incubated in capacitating HTF medium in the absence (control) or presence of increasing concentrations of mSEMG1 (1, 3, 10, and 25 μM). Sperm motility and viability were assessed after 20 and 120 min. Dots with the same color represent the values from an independent experiment. Asterisks indicate statistically significant differences from the control group ($p<0.05$, ANOVA followed by Dunnett´s test). Percentage data were transformed using arcsine square-root values before statistical analysis. Results are presented as mean ± SEM values from independent experiments using sperm samples from 3-7 mice.

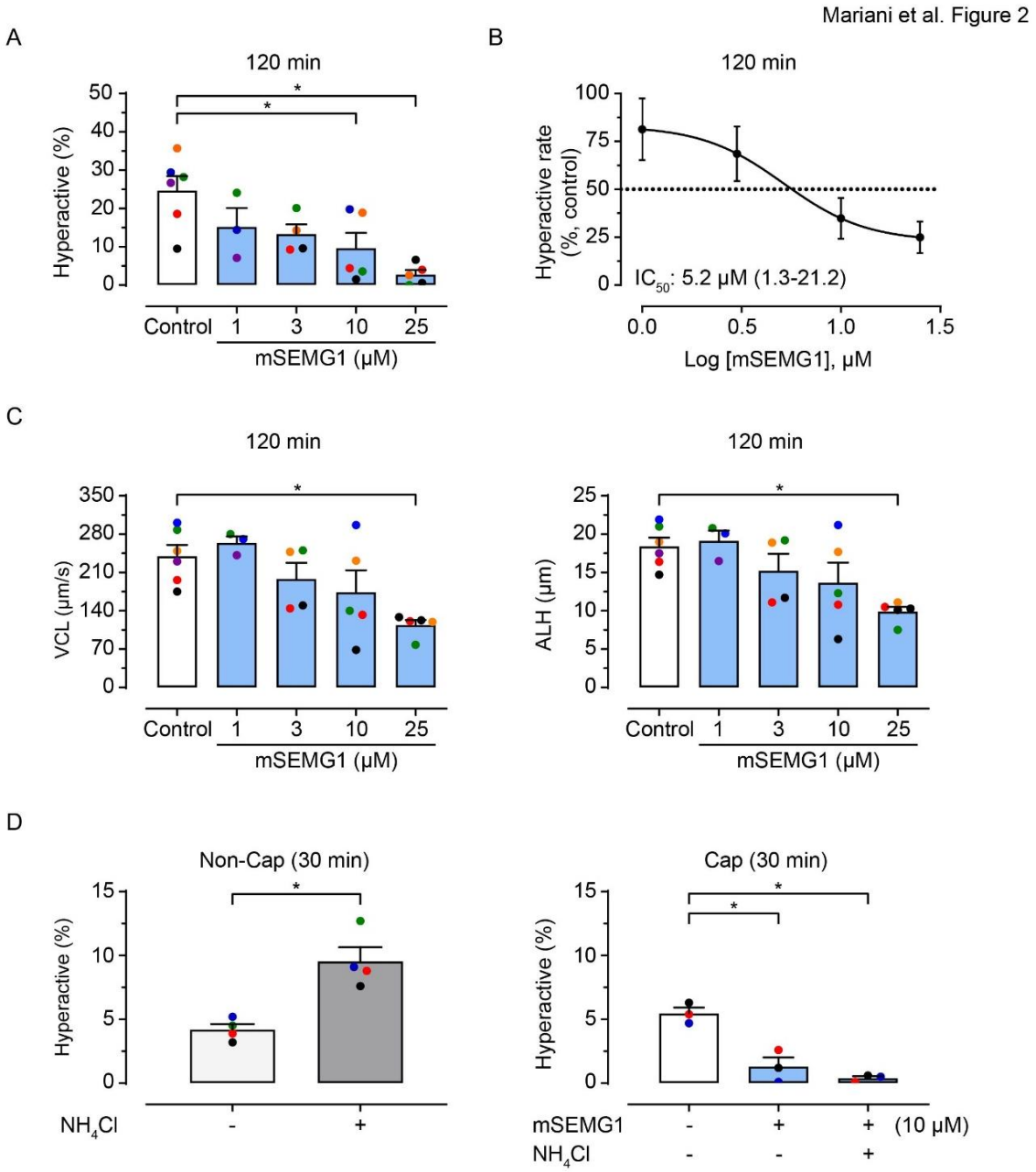

Figure 2. Effects of recombinant mouse semenogelin-1 (mSEMG1) on hyperactivated sperm motility. A, Percentage of hyperactivated motility of spermatozoa after incubation with mSEMG1. **B,** Mean concentration-response curve of hyperactivated motility rate of spermatozoa after incubation with mSEMG1. Data were expressed as percentage values relative to the control group. Inhibitory concentration 50% (IC_{50}, 95% confidence interval) is presented. **C,** Curvilinear velocity (VCL) and amplitude of lateral head displacement (ALH) of spermatozoa after incubation with mSEMG1. Spermatozoa were isolated from the cauda epididymidis and incubated in capacitating HTF medium in the absence (control) or presence of increasing concentrations of mSEMG1 (1, 3, 10, and 25 μM). **D,** Percentage of hyperactivated motility of spermatozoa after incubation with mSEMG1 in the presence or absence of NH_4Cl. Spermatozoa were incubated in non-capacitating TYH medium (Non-Cap), supplemented or not with NH_4Cl (left panel), or in capacitating TYH medium (Cap), supplemented or not with NH_4Cl in the absence or presence of 10 μM mSEMG1 (right panel). Sperm motility was assessed after 30 and 120 min. Dots with the same color represent the values from an independent experiment. Asterisks indicate statistically significant differences from the control group ($p<0.05$, ANOVA followed by Dunnett´s test). Percentage data were transformed using arcsine square-root values before statistical analysis. Results are presented as mean ± SEM values from independent experiments using sperm samples from 3-6 mice.

Mouse SEMG1 is a CatSper channel inhibitor

Activation of the CatSper channel, which leads to a rise in intracellular Ca^{2+} concentration, is essential for the development of hyperactivated motility in both mouse and human spermatozoa (12, 21, 44). Thus, we decided to test the hypothesis that mSEMG1 inhibits hyperactivation by modulating CatSper activation. For that, we conducted whole-cell patch clamp experiments using non-capacitated spermatozoa to detect CatSper currents ($I_{CatSper}$), as previously described (45, 46), in the absence or presence of mSEMG1.

Experiments were performed by ramping the membrane voltage from -80 to +80 mV from a holding potential of 0 mV (Fig. 3A). Under these conditions, no CatSper current was detected in a high-saline (HS) extracellular solution containing Ca^{2+} and Mg^{2+} (Table S1), which represents the baseline recording (Fig. 3B). Upon perfusion with divalent-free Cs^{+}-based (DVF) bath solution (Table S2), the characteristic monovalent CatSper current was recorded (Fig. 3B). Following the DVF perfusion, spermatozoa were exposed to 5 μM mSEMG1, which suppressed both inward and outward CatSper currents (Fig. 3B, C). After subtracting the HS-leak currents, the mean (± standard error of the mean) inward CatSper current at -80 mV was 218.4 ± 31.7 pA for DVF solution only, used as control (Fig. 3B). Under the same conditions, 5 μM mSEMG1 inhibited the inward CatSper current compared to control, with a mean value of 150.8 ± 23.4 pA (~31% suppression; $p = 0.019$) (Fig. 3B). No currents were detected when spermatozoa from *CatSper1*$^{-/-}$ mice were tested either in the absence or presence of mSEMG1 (Fig. 3B, insert). Notably, washing out mSEMG1 recovered CatSper conductance (177.0 ± 17.2 pA; $p = 0.378$) (Fig. 3B), suggesting that its removal from the plasma membrane allows normal CatSper activation.

Besides intracellular pH alkalization, membrane depolarization is another factor that triggers CatSper opening (4, 42). During sperm capacitation, the resulting CatSper activation increases Ca^{2+} influx, which in turn promotes membrane hyperpolarization via the sperm-specific K^{+} channel KSper, a process also dependent on elevated intracellular pH (47). Therefore, we tested whether the reduction of CatSper currents in the presence of mSEMG1 could be associated with changes in membrane potential (Em) during sperm capacitation. As expected, capacitated spermatozoa displayed a lower membrane potential in comparison to non-capacitated spermatozoa (Fig. 3D, Fig. S3). Capacitation-induced membrane hyperpolarization was not affected in the presence of 10 μM mSEMG1 (Fig. 3D, Fig. S3). These results indicate that mSEMG1 inhibits CatSper activity at low micromolar concentrations similar to those required to inhibit sperm hyperactivation, without affecting the Em hyperpolarization during capacitation. In the normal physiological scenario, mouse SEMG1 is present in the seminal plasma at higher concentrations (≥ 25 μM) than its IC_{50} for inhibiting hyperactivation in our experimental conditions (31). Thus, SEMG1 is likely to be able to prevent premature hyperactivation by blocking CatSper activation in mouse spermatozoa, through mechanisms independent of intracellular alkalinization and Em hyperpolarization.

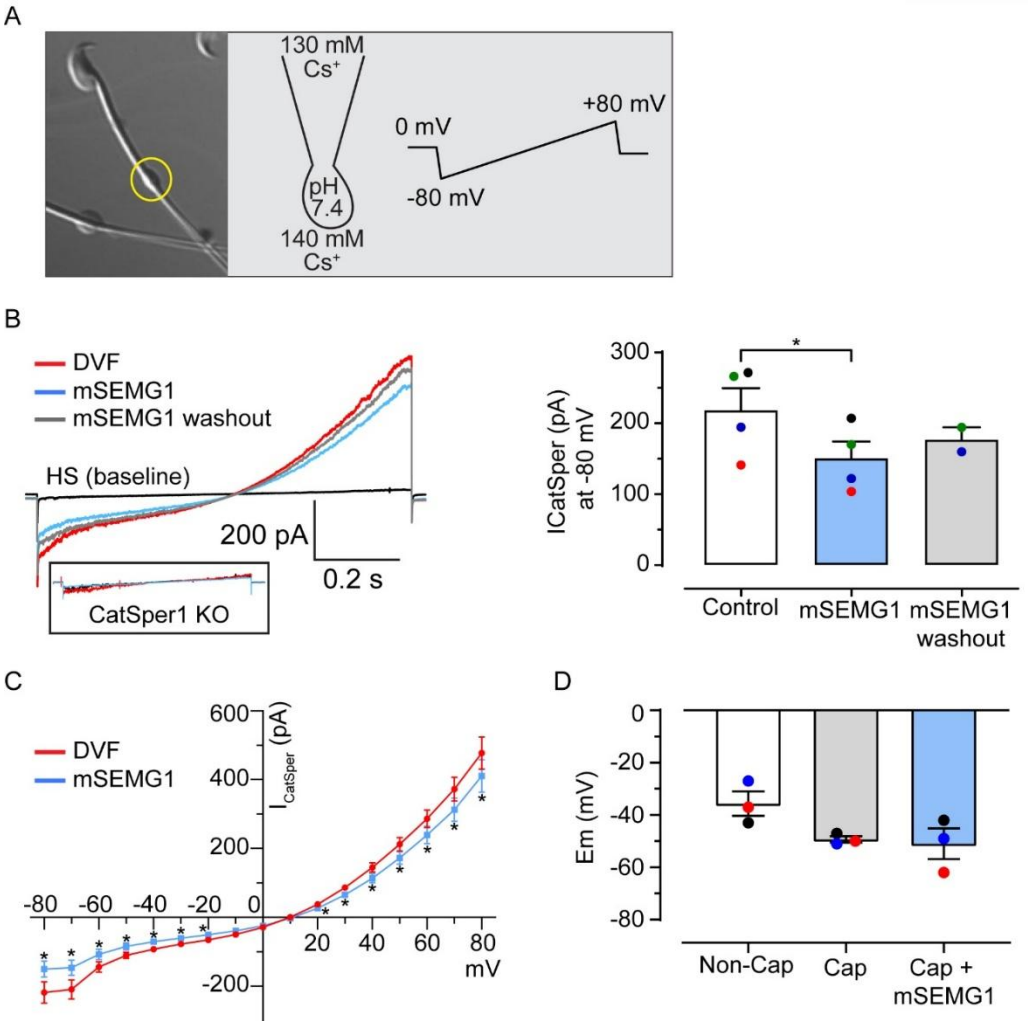

Figure 3. Effects of recombinant mouse semenogelin-1 (mSEMG1) on CatSper currents ($I_{CatSper}$). A, Schematic representation of a spermatozoon with an appropriate cytoplasmic droplet (yellow circle) for patch-clamp recording. The Cs^+ concentration and pH of the pipette and bath solutions are shown. Voltage ramps (-80 mV to 80 mV, 1 s) were applied in a high-saline solution (HS) and a nominally divalent-free solution (DVF) for $I_{CatSper}$ recordings. Baseline currents are recorded in HS solution, which produces no CatSper current due to inhibition by high extracellular magnesium. **B,** Left: $I_{CatSper}$ recordings in response to voltage ramps in DVF solution before and after 5 µM mSEMG1, recorded from wild-type and CatSper KO (inset) mouse spermatozoa. Voltage ramps were measured again in DVF solution after mSEMG1 was washed out. DVF solution: red; HS solution: black; mSEMG1: blue; mSEMG1 washout: grey. Traces represent recordings from the same spermatozoon. Right: $I_{CatSper}$ recordings (mean ± SEM; pA) obtained at −80 mV in DVF solution before and after 5 µM mSEMG1. $I_{CatSper}$ recording was repeated in DVF after mSEMG1 was washed out. Sperm cell capacitance ranged from 2.0 to 2.6 pF. Dots with the same color represent current values from the same spermatozoon. **C,** Current-voltage (I-V) relationships were calculated from amplitudes shown in panel A in the DVF solution before and after 5 µM mSEMG1 treatment. **D,** Quantification of membrane potential (Em) in non-capacitated, capacitated, and capacitated spermatozoa treated with 10 µM mSEMG1. Dots with the same color represent values from independent experiments. Asterisks indicate statistically significant differences from the control group ($p < 0.05$, ANOVA followed by Dunnett's test or paired t-test). Results are presented as mean ± SEM from independent experiments using sperm samples from 3-4 mice.

Mouse SEMG1 Q32-V118 and R98-S220 sequences independently contribute to the inhibition of sperm hyperactivation and CatSper currents

Despite the low conservation in their primary sequences, both human and mouse SEMG1 exhibit a single cysteine residue (Cys239 in human SEMG1 and Cys97 in mouse SEMG1), as well as internal repetitive amino acid sequences (48). Downstream of the cysteine residue, mouse SEMG1 contains two 31-amino acid repeats (K119-S149 and K177-S207) and multiple short repeats of two (KS), three (GGS), or six-eight (QVKSSVSQ or QVKSSGSQ) amino acid residues that become less frequent toward its C-terminal region (Fig. 4A). Previous studies demonstrated that sequences within human SEMG1 that are part of long repeats and flank the cysteine residue are essential for its interaction with spermatozoa, EPPIN binding, and modulation of sperm motility (30, 41). Based on these observations, we commercially obtained three truncated mSEMG1 constructs (i) mSEMG1$^{Q32-V118}$, which contains its unique cysteine residue, (ii) mSEMG1$^{R98-G375}$, which lacks the cysteine residue but includes the two long repeats, and (iii) mSEMG1$^{Y220-G375}$, which lacks both the cysteine residue and the long repeats (Fig. 4A), allowing us to evaluate the relevance of these sequences to the inhibition of sperm hyperactivation.

We observed that no truncated mSEMG1 construct affected sperm motility in a significant manner (Fig. 4B). Nevertheless, mSEMG1$^{Q32-V118}$ and mSEMG1$^{R98-G375}$, but not mSEMG1$^{Y220-G375}$, inhibited hyperactivated motility ($p = 0.004$ and 0.028, respectively) to a similar extent as the full-length mSEMG1 (Fig. 4B-C, Fig. S4, Video S2). mSEMG1$^{Q32-V118}$ also reduced the associated kinematic parameter VCL ($p = 0.029$), and a similar trend was observed for mSEMG1$^{R98-G375}$ ($p = 0.084$) (Fig. 4C). Consistent with these findings, both mSEMG1$^{Q32-V118}$ and mSEMG1$^{R98-G375}$ suppressed inward and outward CatSper currents (Fig. 5A, B, and Fig. S5). mSEMG1$^{Y220-G375}$ also inhibited CatSper currents, albeit to a lesser extent than the other truncated constructs (Fig. 5A, B, Fig. S5). At 5 μM concentration, mSEMG1$^{Q32-V118}$, mSEMG1$^{R98-G375}$, and mSEMG1$^{Y220-G375}$ suppressed the inward CatSper current at -80 mV to values equivalent to 56%, 66%, and 77% of those observed with their respective controls, corresponding to mean differences of of 93.6 ($p = 0.007$), 108.6 ($p < 0.0001$), and 55.9 pA ($p = 0.011$), respectively (Fig. 5A, Fig. S5). These results indicate that sequences within the mSEMG1 Q32-V118 and R98-S220 regions, which encompass cysteine and the long repeats, respectively, contain domains that are sufficient to inhibit sperm hyperactivation through CatSper inhibition.

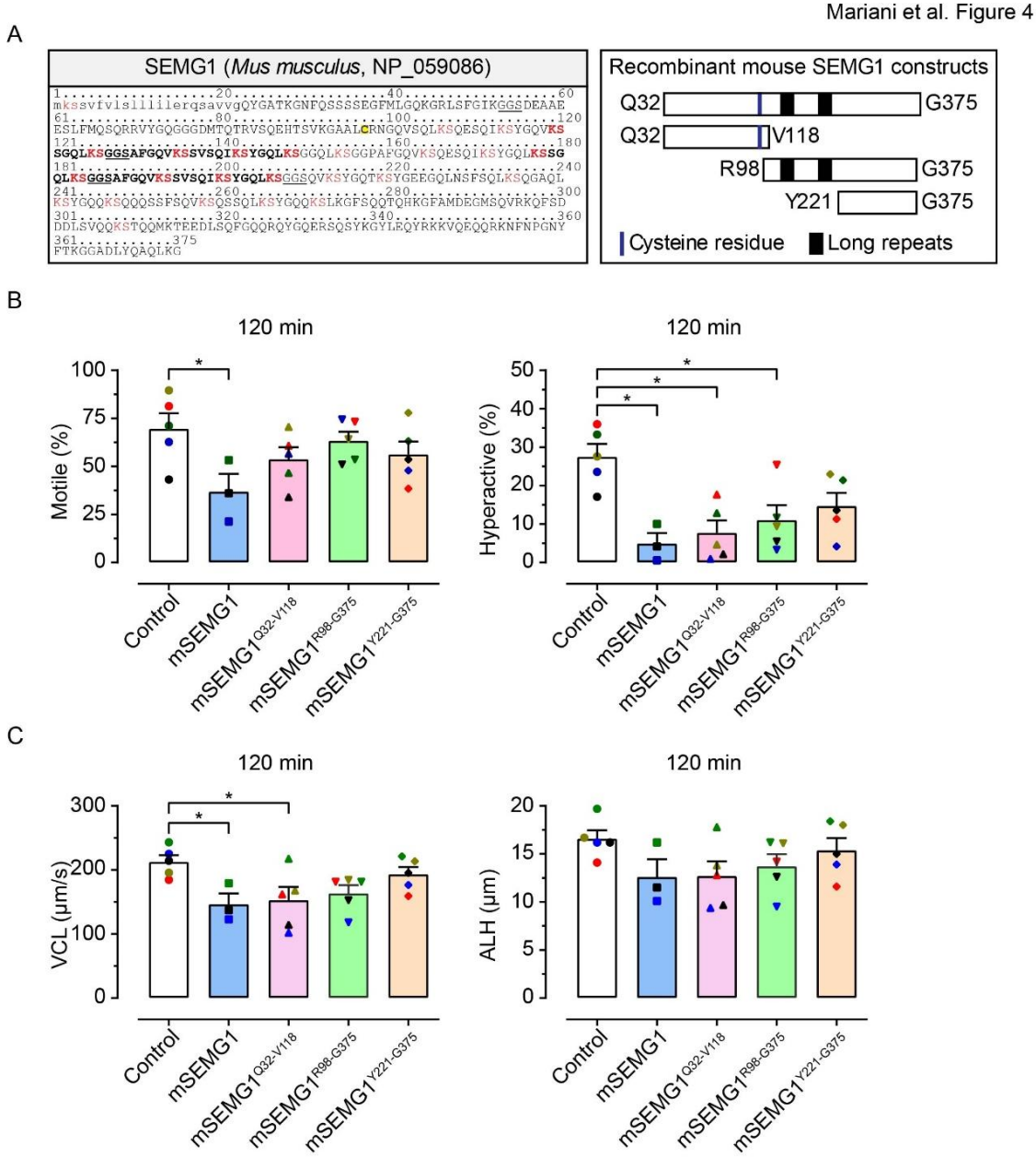

Figure 4. Mouse SEMG1 sequence, recombinant constructs, and their effects on sperm motility. A, Left: Primary amino acid sequence of mouse SEMG1. The signal peptide is shown in lowercase letters. Amino acid repeats are indicated in bold. The GGS region is underlined, while the KS region and the single cysteine residue are highlighted in red and yellow, respectively. Right: Schematic representation of recombinant mouse semenogelin-1 (mSEMG1) full-length and truncated constructs used in the experiments. The mSEMG1 constructs include a 6x-His tag. **B,** Percentage of total (left) and hyperactivated (right) motility of spermatozoa after incubation with mSEMG1. **C-D,** Curvilinear velocity (VCL) (C) and amplitude of lateral head displacement (ALH) (D) of spermatozoa after incubation with mSEMG1 constructs. Spermatozoa were isolated from the cauda epididymidis and incubated in capacitating HTF medium in the absence (control) or presence of mSEMG1 constructs (25 µM). Sperm motility was assessed after 120 min. Dots with the same color represent the values from an independent experiment. Asterisks indicate statistically significant differences from the control group ($p<0.05$, ANOVA followed by Dunnett´s test). Percentage data were transformed using arcsine square-root values before statistical analysis. Results are presented as mean ± SEM values from independent experiments using sperm samples from 3-5 mice.

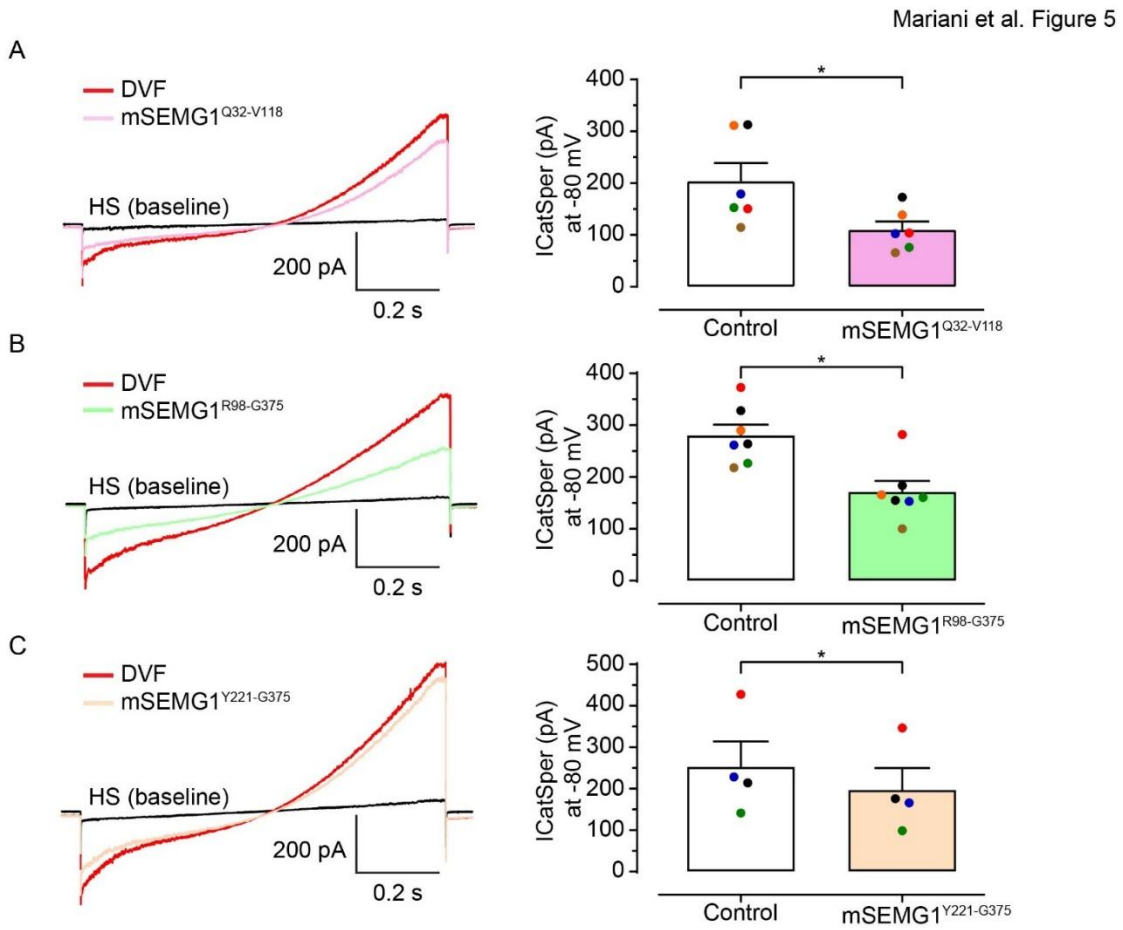

Figure 5. Effects of recombinant mouse semenogelin-1 (mSEMG1) fragments on CatSper currents ($I_{CatSper}$). A-C, Left: Representative $I_{CatSper}$ recordings in response to voltage ramps in divalent-free solution (DVF) before and after 5 µM mSEMG1$^{Q32–V118}$ (A), mSEMG1$^{R98–G375}$ (B), and mSEMG1$^{Y221–G375}$ (C), recorded from wild-type mouse spermatozoa. Baseline currents are recorded in high-saline solution (HS), which produces no CatSper current due to inhibition by high extracellular magnesium. Traces represent recordings from the same spermatozoon. DVF solution: red; HS solution: black; mSEMG1: blue; mSEMG1 washout: grey. Right: Quantification of $I_{CatSper}$ (mean ± SEM; pA) at −80 mV in DVF solution before and after addition of the respective mSEMG1 fragments. Sperm cell capacitance ranged from 2.1 to 2.8 pF. Dots with the same color represent values from independent experiments. Asterisks indicate statistically significant differences from the control group ($p < 0.05$, paired t-test). Results are presented as mean ± SEM from independent experiments using sperm samples from 4-7 mice.

Mouse SEMG1 R98-G220 sequence contains the main EPPIN binding domain

Our previous study demonstrated the co-immunoprecipitation and co-localization of SEMG1 and EPPIN in mouse spermatozoa pre-incubated with seminal vesicle fluid, suggesting that EPPIN serves as a docking site for SEMG1 on the mouse sperm surface (26). Here, we confirmed the interaction between mouse EPPIN and SEMG1 using the AlphaScreen (Amplified Luminescent Proximity Homogeneous Assay Screen) assay (Fig. 6A), which has been previously employed to investigate the binding of human EPPIN and SEMG1 (27, 41). Using mSEMG1 and full-length recombinant mouse EPPIN (mEPPIN; L24-T134), we observed a maximum interaction signal peaking at 2 hrs and remaining stable for at least 8 hrs (Fig. 6B). The interaction signals showed a concentration-dependent pattern when mSEMG1 and mEPPIN were titrated, with calculated EC_{50} (95% CI) of 23.6 nM (20.0-27.8 nM) and 1.0 nM (0.3-3.3 nM), respectively (Fig. 6C). Interestingly, when recombinant human SEMG1 (hSEMG1, G26-R281) replaced mSEMG1, we observed a concentration-dependent saturable binding curve, with a calculated EC_{50} of 11.2 nM (6.8-18.5 nM), confirming the conservation of the EPPIN binding sites in human and mouse SEMG1 sequences (Fig. S6).

To map the EPPIN binding site, we tested the mEPPIN binding capacity of our truncated mSEMG1 constructs. $mSEMG1^{R98-G375}$ showed a mEPPIN binding capacity similar to the full-length mSEMG1, both displaying a comparable specific signal (Fig. 6D). In contrast, we observed a reduction in the specific signal by ~80% ($p < 0.0001$) and 69% ($p < 0.0001$) for $mSEMG1^{Q32-V118}$ and $mSEMG1^{Y220-G375}$ in comparison to full-length mSEMG1, respectively (Fig. 6D).

In addition, the removal of mouse EPPIN Kunitz domain in a C-terminal truncation lacking residues C69-T134 resulted in a reduction in the specific signal by ~75% ($p = 0.001$) compared to that detected with full-length EPPIN (Fig. 6E). Competition assays using anti-EPPIN antibodies Q20E and S21C, that recognized epitopes within EPPIN WFDC and Kunitz domains, respectively, reduced the specific signal of the binding of mEPPIN and mSEMG1 in a concentration-dependent manner with IC_{50} values of 3.0 nM (0.2-34.3 nM) and 95.6 nM (20.6-443.6 nM), respectively (Fig. S7). Altogether, these results demonstrate that the sequence R98-S220 of mSEMG1 contains the major mEPPIN binding domain and that both WFDC and Kunitz domains of mEPPIN are involved in mSEMG1 binding.

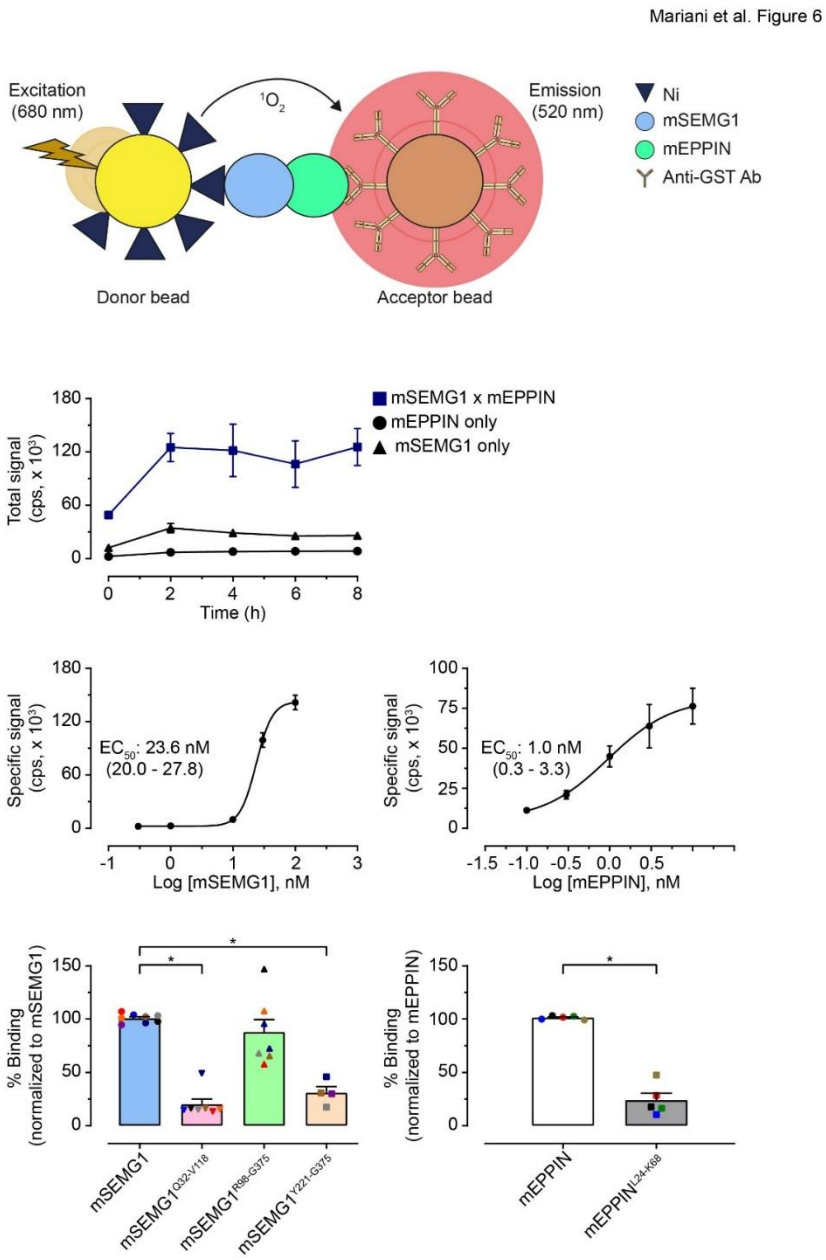

Figure 6. Characterization of the interaction between recombinant mouse semenogelin-1 (mSEMG1) and recombinant mouse EPPIN (mEPPIN). A, Schematic representation of the AlphaScreen assay. GST-tagged mEPPIN was captured by anti-GST acceptor beads, and 6×His-tagged mSEMG1 by Ni^{2+}-chelate donor beads. Upon excitation at 680 nm, a luminescent signal was generated due to the proximity (<200 nm) of donor and acceptor beads, indicating an interaction between mEPPIN and mSEMG1. **B,** mEPPIN was incubated with mSEMG1 in a time-course experiment. Background signal was detected when beads were incubated in the absence of mEPPIN or mSEMG1. Data are presented as mean ± SEM from a representative experiment out of ten, each performed in triplicate. **C,** Left: Concentration-response curve for mSEMG1 with a constant concentration of mEPPIN (10 nM). Right: Concentration-response curve for mEPPIN with a constant concentration of mSEMG1 (30 nM). A specific signal for each data point was determined by subtracting the background signal from the total signal. Results represent mean ± SEM of specific signals from 2-4 experiments. **D,** Left: mSEMG1 and its fragments (Q32-V118: $mSEMG1^{Q32-V118}$, R98-G375: $mSEMG1^{R98-G375}$, and Y221-G375: $SEMG^{Y221-G375}$) were incubated with mEPPIN for 4 hours. Right: mEPPIN and its N-terminal construct (L24-K68: $mEPPIN^{L24-K68}$) were incubated with mSEMG1 for 4 hours. Dots with the same color represent values from independent experiments. Specific signals for each data point were normalized as a percentage of the signal from full-length mSEMG1/mEPPIN binding. Asterisks indicate statistically significant differences from the control group (mSEMG1 or mEPPIN) ($p<0.05$, ANOVA followed by Dunnett´s test). Results are expressed as mean ± SEM of specific signals from 4-10 experiments. Cps = counts per second.

Discussion

Upon ejaculation, SEMG1 coats the sperm surface by interacting with EPPIN (26, 27, 41), thereby modulating sperm motility and several capacitation-associated events, such as hyperactivation and acrosome exocytosis (30, 31, 33, 39, 49). However, the underlying mechanisms governing the effects of SEMG1 on sperm function remain elusive. Here, we demonstrate that mSEMG1 inhibited sperm hyperactivation at concentrations at least 200-fold lower than those previously reported (33), highlighting SEMG1 as a potent, endogenous inhibitor of sperm hyperactivation. Moreover, we reveal that mouse SEMG1 contains two distinct functional domains – within the Q32-V118 and R98-S220 sequences – which inhibit sperm hyperactivation by targeting CatSper at physiological concentrations. Since only the R98-S220 sequence is required for EPPIN binding, our data indicate that SEMG1 operates through both EPPIN-dependent and independent mechanisms to regulate sperm hyperactivation.

During capacitation, spermatozoa experience a pH_i shift from acidic to alkaline, primarily driven by Na^+/H^+ exchangers (NHEs) in mice (50, 51). This event is crucial for the activation of sperm-specific ion channels, such as CatSper, which in turn leads to a rise in $[Ca^{2+}]_i$ (5, 14). Ca^{2+} influx through CatSper plays a fundamental role in reproduction, as the channel dysfunction leads to male infertility associated with hyperactivation failure in both humans and mice (52). While previous reports have demonstrated that the inhibition of sperm motility by SEMG1 was related to a decrease in $[Ca^{2+}]_i$ (39), the direct association of CatSper in this process has not been clarified. As shown herein, mSEMG1 exerts inhibitory effects on hyperactivation through inhibition of CatSper currents, thereby revealing a novel regulatory mechanism for CatSper activity promoted by a seminal plasma protein.

Given that intracellular alkalization is a well-established trigger for CatSper activation and downstream signaling (42), we investigated whether pharmacologically induced pH_i increase could rescue sperm hyperactivation following mSEMG1 treatment. Our findings showed that hyperactivation remained suppressed despite pH_i alkalization, indicating a downstream effect. It is worth noting that $[Ca^{2+}]_i$ increase during capacitation contributes to Em hyperpolarization and intracellular alkalinization, forming a positive feedback loop that in turn potentiates CatSper activity (51, 53). In this regard, Em hyperpolarization is mediated by KSper, which localizes along the sperm flagellum (47, 54). mSEMG1 did not alter Em hyperpolarization during sperm capacitation, indicating that it does not affect KSper activity. These observations support the conclusion that SEMG1-mediated CatSper inhibition occurs independently of pH_i or Em changes. Therefore, further studies are needed to determine whether SEMG1 binds directly to CatSper subunits or interferes indirectly with channel activation, secondary to protein-protein interactions or inhibition of specific signaling pathways. One putative mechanism involves the ability of SEMG1 to stabilize membrane microdomains through modulation of cholesterol removal and binding to lipid raft components, such as the ganglioside GM1 (55), which may in turn affect capacitation-associated membrane

modifications and modulate CatSper activity. Further experimental evidence is required to test this hypothesis.

Our findings identified two domains within the mSEMG1 Q32-V118 and R98-S220 sequences that play crucial roles in inhibiting sperm hyperactivation. Consistently, truncated constructs containing these sequences promoted inhibition of CatSper activity to a similar extent as the full-length mSEMG1. These findings are consistent with previous observations that SEMG1 is a modular protein, containing distinct domains that independently contribute to its multifunctional roles in sperm function and protection (48). Physiologically, SEMG1 associates with the sperm surface through binding to EPPIN, an event that is crucial for the inhibition of sperm motility in the semen coagulum (30, 34, 39). Our previous results demonstrated the co-immunoprecipitation of EPPIN and SEMG1 from mouse spermatozoa incubated with the seminal vesicle fluid when either anti-EPPIN or anti-SEMG1 antibodies were used, indicating a parallel system to humans (26). Thus, we decided to investigate the relevance of EPPIN binding to the effects of mSEMG1 on sperm function. First, we showed that mouse EPPIN and SEMG1 are binding partners, confirming that EPPIN is a docking site for SEMG1 on the mouse sperm surface (26). The functional conservation of EPPIN as a sperm-associated hub for SEMG1 binding in both humans and mice was further demonstrated by the capacity of mouse EPPIN to bind human SEMG1. Moreover, we identified the mSEMG1 R98-S220 sequence, which lacks its unique cysteine residue but encompasses two long amino acid repeats, as containing the major EPPIN binding domain. This result was unexpected, since human SEMG1 relies on amino acid sequences flanking its unique cysteine residue to bind EPPIN and inhibit sperm motility (41). Likely, the rapid adaptive evolution pattern of the human *SEMG1* and mouse *Semg1* genes could play a role in shifting the EPPIN binding site to different pockets in its primary sequence (41). Altogether, our results led us to conclude that mouse SEMG1 may inhibit sperm hyperactivation through both EPPIN-dependent and independent mechanisms.

Based on our findings, we propose a working model by which SEMG1 regulates hyperactivation in ejaculated spermatozoa in mice (Fig. 7). Upon ejaculation, SEMG1 coats the surface of spermatozoa at least in part through EPPIN binding, preventing premature hyperactivation and capacitation within the female reproductive tract. This event is mediated by two distinct SEMG1 domains within Q32-V118 and R98-S220 sequences that independently inhibit CatSper activity. In the upper regions of the female reproductive tract, a putative PSA-like protease (likely belonging to the kallikrein family) cleaves SEMG1, allowing spermatozoa to undergo hyperactivation and capacitation. Collectively, these findings position SEMG1 Q32-V118 and R98-S220 sequences as compelling prototypes for the rational design of CatSper inhibitors with potential applications in male contraception targeting critical regulatory pathways for hyperactivation.

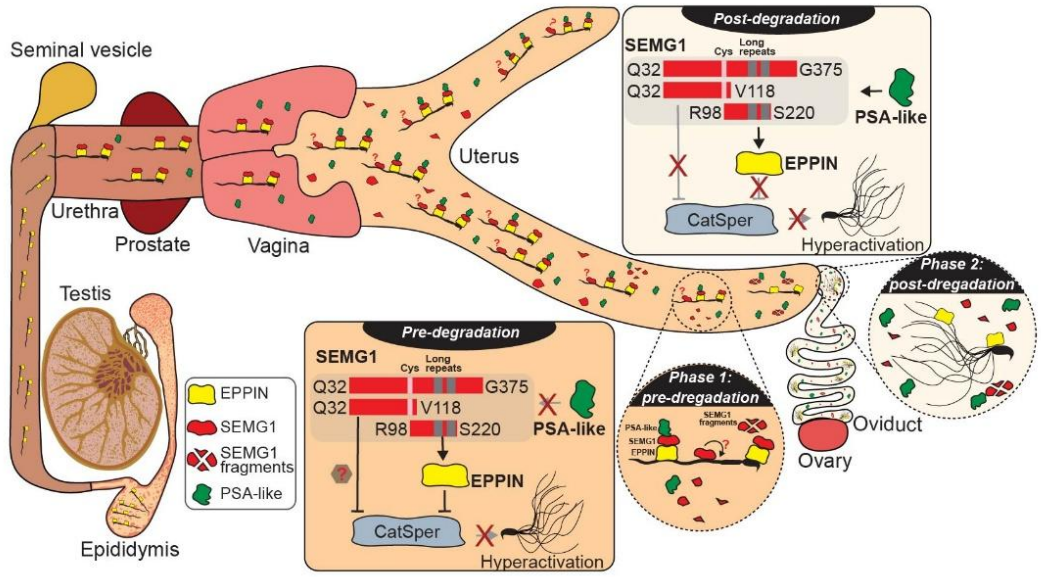

Figure 7. Working model of SEMG1-mediated inhibition of sperm hyperactivation after sperm ejaculation. EPPIN is present on the surface of mature spermatozoa stored in the cauda epididymidis. After ejaculation, the seminal plasma protein SEMG1 binds to the sperm surface via interaction with EPPIN through a binding domain within residues R98-S220, thus coating spermatozoa. SEMG1 may also interact with spermatozoa independently of EPPIN binding. During sperm transit through the female reproductive tract, the Q32-G375 and R98-S220 SEMG1 domains exert inhibitory effects on sperm function, temporarily preventing hyperactivation in the uterus by inhibiting CatSper, while only the R98-S220 domain contains the EPPIN binding site (Phase 1; Pre-dregadation phase). As spermatozoa move to the upper regions of the female reproductive tract, SEMG1 is proteolytically cleaved by a PSA-like enzyme, whose identity remains unknown in mice, allowing hyperactivation to take place in the oviduct.

Experimental Procedures

Animals

We used male (90–120 days old) and female (60–90 days old) Swiss mice obtained from the Center for Research and Production of Laboratory Animals (CPPA) of São Paulo State University (UNESP), Botucatu, São Paulo, Brazil. The animals were maintained under controlled conditions (12 h light/dark cycle, 22–24 °C) with food and water available ad libitum. All procedures were approved by the Animal Care and Use Committee of UNESP (protocol #5219150420) and followed the guidelines of the Brazilian National Council for the Control of Animal Experimentation (CONCEA). We also used wild-type (WT) and CatSper1-deficient male C57BL/6 mice, maintained at the Animal Facility of Washington University in St. Louis (USA) and the Facultad de Ciencias Bioquímicas y Farmacéuticas, Universidad Nacional de Rosario (Argentina). These animals were used for patch-clamp recordings, membrane potential analysis, and additional sperm motility experiments. All experiments were conducted following the institutional guidelines for animal research and were approved by the respective Animal Care and Use Committees. Mice were euthanized by inhaled isoflurane overdose or CO_2 inhalation, followed by cervical dislocation.

Protein-protein interaction assays

We performed AlphaScreen to evaluate protein–protein interactions, following the protocol described by (41), with the modifications detailed below. Briefly, recombinant mEPPIN and its N-terminal fragment, both containing an N-terminal TGST tag, were pre-incubated with anti-GST acceptor beads for 60 minutes. In parallel, mSEMG1 and its truncated fragments (Fig. 4A), containing a 6x-his tag, were incubated with Ni-NTA-chelate donor beads under the same conditions. Equal volumes of the mEPPIN/acceptor bead suspension and the mSEMG1/donor bead suspension were transferred to white opaque 384-well microplates (OptiPlate-384; PerkinElmer, Waltham, MA), in a final reaction volume of 30 µL per well. Plates were sealed and placed in a Synergy 2 Multiplatform automated plate reader (BioTek, Winooski, VT). After 2 minutes of shaking, readings were taken every 2 hrs over 8 hrs, using a 680/30 excitation filter and a 570/100 emission filter. Data acquisition was performed using Gen5 software (BioTek), and a total of 9 time points were recorded per experiment. All conditions were assayed in triplicate.

Final concentrations of the assay components ranged from 0.1–10 nM for mEPPIN, 0.3–100 nM for mSEMG1, and 10 µg/mL for the donor and acceptor beads. Negative controls were conducted under the same conditions in the absence of either mEPPIN or mSEMG1, with beads only. The specific signal at each time point was calculated by subtracting the background signal (obtained in the absence of one of the proteins) from the total signal. To determine the EC_{50} for mEPPIN binding to mSEMG1, we applied nonlinear regression curve fitting to the specific signal values obtained after 4 hrs of incubation. For competition assays, we incubated mEPPIN (10 nM) and mSEMG1 (30 nM) in the presence of increasing concentrations of anti-EPPIN Q20E (targeting the P20–E39 epitope) or anti-EPPIN S21C (targeting the S103–C121 epitope) antibodies, maintaining a total reaction volume of 30 µL and bead concentration at 10 µg/mL. Specific signals for each competitor concentration were calculated as described, and IC_{50} values were determined by nonlinear regression. The expression and purity of mEPPIN and mSEMG1 were confirmed by Western blot before the experiments (Fig. S4).

Analysis of Sperm Motility

We performed analysis of sperm motility following the protocol described by (35), with the modifications detailed below. We collected mouse spermatozoa from the cauda epididymides and incubated them in human tubal fluid (HTF) medium at 37 °C under 5% CO_2. After 10 minutes of incubation, we removed the tissue and diluted the sperm suspension (~40,000 cells) in HTF supplemented with 25 mM sodium bicarbonate and 0.75% bovine serum albumin (BSA; Sigma, cat. #SLBT1197). We treated the sperm suspensions with recombinant mSEMG1 or its truncated

constructs (1–25 μM) (Fig. 4). Negative controls were prepared using HTF medium without recombinant proteins. Rescue experiments were performed to assess whether intracellular alkalinization could counteract the inhibitory effects of mSEMG1 on sperm motility. Alkalinization was induced by NH_4Cl addition, and its efficacy was verified by analyzing sperm motility under non-capacitating conditions (medium lacking bicarbonate and BSA) following NH_4Cl treatment. Sperm motility was analyzed using a computer-assisted sperm analysis (CASA) system (Hamilton-Thorne, Beverly, MA, USA) with Animal Motility II Software version 1.9. We acquired images using an Olympus CX41 microscope equipped with a MiniTherm stage warmer and a JAI CM-040 digital camera. Aliquots of the sperm suspensions were loaded into pre-warmed 80-μm 2X-CEL slides (Hamilton-Thorne) at 37 °C using large-bore pipette tips. We assessed sperm motility at 30, 60, and 120 minutes after incubation. Time zero was defined as 2 minutes after the addition of anti-EPPIN antibodies.

We recorded sperm tracks for 1.5 s (90 frames) at a frame rate of 60 Hz using a 40× negative-phase contrast objective. For each sample, we analyzed at least 200 spermatozoa across 10 different fields. We used video playback to review and manually correct the tracks, removing mistracked cells caused by collisions or debris interference. We then extracted individual ASCII files containing the kinematic parameters for each sperm cell. The following parameters were analyzed: average path velocity (VAP, mm/s), straight-line velocity (VSL, mm/s), curvilinear velocity (VCL, mm/s), amplitude of lateral head displacement (ALH, μm), straightness (STR, %), and linearity (LIN, %). We classified sperm as progressive when VAP > 50 mm/s and STR > 50%, hyperactivated when VCL > 180 mm/s, ALH > 9.5 μm, and LIN < 23.6%, and slow when VAP ≤ 30 μm/s and VSL ≤ 20 μm/s.

Electrophysiology

We performed electrophysiological recordings as described by (46). Gigaohm seals were established at the cytoplasmic droplet of mouse sperm (Fig. 3) using a High-Saline (HS) solution containing (in mM): 130 NaCl, 5 KCl, 1 $MgSO_4$, 2 $CaCl_2$, 5 glucose, 1 sodium pyruvate, 10 lactic acid, and 20 HEPES (pH 7.4). We achieved whole-cell configuration by applying brief (1 ms) voltage pulses of 400–630 mV combined with gentle suction. To elicit currents, we applied voltage ramps from −80 mV to +80 mV, starting from a holding potential of 0 mV, in both HS and a nominally divalent-free (DVF) bath solution. Data were acquired at a sampling rate of 2–5 kHz and low-pass filtered at 1 kHz. Patch pipettes (11–17 MΩ) were filled with an internal solution containing (in mM): 130 Cs-methanesulfonate, 70 HEPES/MES, 3 EGTA, 2 EDTA, and 0.5 Tris-HCl (pH adjusted to 7.4 with CsOH). The DVF bath solution used for recording monovalent CatSper currents contained (in mM): 140 Cs-methanesulfonate, 40 HEPES/MES, and 1 EDTA (pH 7.4). We recorded baseline currents in HS before switching to DVF. To evaluate the effects of mSEMG1 and its fragments, we

added the proteins (5 or 10 μM; 400–500 μL), diluted in DVF, in real-time during the recordings. The complete compositions of the HS, DVF, and pipette solutions are listed in Tables S1, S2, and S3. All recordings were conducted at Washington University in St. Louis, MO, USA.

Statistical Analysis

Data are presented as mean ± SEM. Normality and homoscedasticity were assessed using the Kolmogorov–Smirnov test and F-test, respectively. Statistical differences between two independent groups were analyzed using an unpaired Student's t-test; for comparisons involving more than two groups, one-way ANOVA followed by Dunnett's post hoc test was used. For electrophysiological recordings, a paired Student's t-test was applied. Percentage data were arcsine square root transformed before statistical analysis. A p-value < 0.05 was considered statistically significant.

Data availability

All data are available in the main text or the supporting information.

Supporting information

This article contains supporting information.

Acknowledgments

We thank Luiz Oliveira, Paulo Mioni, and Flávia Colenci, Ph.D. Department of Biophysics and Pharmacology, IBB/UNESP, for their technical assistance. We are also grateful to Michael O´Rand, Ph.D., and Katherine Hamil, M.Sc., for the critical reading of the manuscript and valuable insights, and Célio Fernandes for his helpful discussions during the project.

Author contributions

Mariani NAP and Silva EJR conceptualization; Mariani NAP, Steeman TJ, Novero AG, Lima JC, Krapf D, Lishko P, Silva EJR methodology; Mariani NAP, Santos NCM and Silva EJR formal analysis; Mariani NAP, Santos NCM, Andrade AD, Santos BR, Andrade JJ, Steeman TJ, Novero AG, Calderaro G, Themer ACF, Kushima H investigation; Silva EJR, Lishko P, and Krapf D resources; Mariani NAP and Silva EJR writing-original draft; Mariani NAP, Lishko P, Krapf D, Buffone MG, and Silva EJR writing–review & editing; Mariani NAP, Santos NCM, Andrade AD, and Silva EJR visualization; Silva EJR, Lishko P, Krapf D and Buffone MG supervision. All authors have read and agree with the final version of the manuscript.

Funding and additional information

This study was funded by São Paulo Research Foundation (FAPESP, grants 2020/04841-3, 2021/04746-3, 2021/06718-7, 2022/10159-6, 2023/00125-0, and 2023/04496-2), Coordenação de Aperfeiçoamento de Pessoal de Nível Superior (CAPES, grants 88887.496465/2020-00 and 88887.657625/2021-00), and Conselho Nacional de Desenvolvimento Científico e Tecnológico (CNPq, grants 303616/2022-9, 442218/2023-0, and 201112/2024-8).

Conflict of Interest

The authors declare that they have no conflict of interest.

References

1. Freitas, M. J., Vijayaraghavan, S., and Fardilha, M. (2017) Signaling mechanisms in mammalian sperm motility. *Biol. Reprod.* **96**, 2–12
2. Stival, C., Puga Molina, L. del C., Paudel, B., Buffone, M. G., Visconti, P. E., and Krapf, D. (2016) Sperm capacitation and acrosome reaction in mammalian sperm. *Adv. Anat. Embryol. Cell Biol.* **220**, 93–106
3. Austin, C. R. (1952) The 'capacitation' of the mammalian sperm. *Nature*. **170**, 326–326
4. Vyklicka, L., and Lishko, P. V. (2020) Dissecting the signaling pathways involved in the function of sperm flagellum. *Curr. Opin. Cell Biol.* **63**, 154–161
5. Ritagliati, C., Baro Graf, C., Stival, C., and Krapf, D. (2018) Regulation mechanisms and implications of sperm membrane hyperpolarization. *Mech. Dev.* **154**, 33–43
6. Witte, T. S., and Schäfer-Somi, S. (2007) Involvement of cholesterol, calcium and progesterone in the induction of capacitation and acrosome reaction of mammalian spermatozoa. *Anim. Reprod. Sci.* **102**, 181–193
7. Visconti, P. E., Westbrook, V. A., Chertihin, O., Demarco, I., Sleight, S., and Diekman, A. B. (2002) Novel signaling pathways involved in sperm acquisition of fertilizing capacity. *J. Reprod. Immunol.* **53**, 133–150
8. López-González, I., Torres-Rodríguez, P., Sánchez-Carranza, O., Solís-López, A., Santi, C. M., Darszon, A., and Treviño, C. L. (2014) Membrane hyperpolarization during human sperm capacitation. *Mol. Hum. Reprod.* **20**, 619–629
9. Suarez, S. S., and Dai, X. (1992) Hyperactivation enhances mouse sperm capacity for penetrating viscoelastic media. *Biol. Reprod.* **46**, 686–691
10. Suarez, S. S., Katz, D. F., Owen, D. H., Andrew, J. B., and Powell, R. L. (1991) Evidence for the function of hyperactivated motility in sperm. *Biol. Reprod.* **44**, 375–381
11. Suarez, S. S. (1987) Sperm transport and motility in the mouse oviduct: observations in situ. *Biol. Reprod.* **36**, 203–210
12. Quill, T. A., Sugden, S. A., Rossi, K. L., Doolittle, L. K., Hammer, R. E., and Garbers, D. L. (2003) Hyperactivated sperm motility driven by CatSper2 is required for fertilization. *Proc. Natl. Acad. Sci. U. S. A.* **100**, 14869–14874
13. Darszon, A., Nishigaki, T., Beltran, C., and Treviño, C. L. (2011) Calcium channels in the development, maturation, and function of spermatozoa. *Physiol. Rev.* **91**, 1305–1355
14. Lishko, P. V., and Mannowetz, N. (2018) CatSper: a unique calcium channel of the sperm flagellum. *Curr. Opin. Physiol.* **2**, 109–113
15. Hwang, J. Y., Mannowetz, N., Zhang, Y., Everley, R. A., Gygi, S. P., Bewersdorf, J., Lishko, P. V., and Chung, J.-J. (2019) Dual sensing of physiologic pH and calcium by EFCAB9 regulates sperm motility. *Cell*. **177**, 1480-1494.e19

16. Bystroff, C. (2018) Intramembranal disulfide cross-linking elucidates the super-quaternary structure of mammalian CatSpers. *Reprod. Biol.* **18**, 76–82
17. Lin, S., Ke, M., Zhang, Y., Yan, Z., and Wu, J. (2021) Structure of a mammalian sperm cation channel complex. *Nature*. **595**, 746–750
18. Zhao, Y., Wang, H., Wiesehoefer, C., Shah, N. B., Reetz, E., Hwang, J. Y., Huang, X., Wang, T., Lishko, P. V., Davies, K. M., Wennemuth, G., Nicastro, D., and Chung, J.-J. (2022) 3D structure and in situ arrangements of CatSper channel in the sperm flagellum. *Nat. Commun.* **13**, 3439
19. Chung, J.-J., Shim, S.-H., Everley, R. A., Gygi, S. P., Zhuang, X., and Clapham, D. E. (2014) Structurally distinct Ca(2+) signaling domains of sperm flagella orchestrate tyrosine phosphorylation and motility. *Cell*. **157**, 808–822
20. Avenarius, M. R., Hildebrand, M. S., Zhang, Y., Meyer, N. C., Smith, L. L. H., Kahrizi, K., Najmabadi, H., and Smith, R. J. H. (2009) Human male infertility caused by mutations in the CATSPER1 channel protein. *Am. J. Hum. Genet.* **84**, 505–510
21. Carlson, A. E., Quill, T. A., Westenbroek, R. E., Schuh, S. M., Hille, B., and Babcock, D. F. (2005) Identical phenotypes of CatSper1 and CatSper2 null sperm. *J. Biol. Chem.* **280**, 32238–32244
22. Chung, J.-J., Miki, K., Kim, D., Shim, S.-H., Shi, H. F., Hwang, J. Y., Cai, X., Iseri, Y., Zhuang, X., and Clapham, D. E. (2017) CatSperζ regulates the structural continuity of sperm Ca2+ signaling domains and is required for normal fertility. *eLife*. **6**, e23082
23. Hildebrand, M. S., Avenarius, M. R., Fellous, M., Zhang, Y., Meyer, N. C., Auer, J., Serres, C., Kahrizi, K., Najmabadi, H., Beckmann, J. S., and Smith, R. J. H. (2010) Genetic male infertility and mutation of CATSPER ion channels. *Eur. J. Hum. Genet. EJHG*. **18**, 1178–1184
24. De Jonge, C. (2005) Biological basis for human capacitation. *Hum. Reprod. Update*. **11**, 205–214
25. Chang, M. C. (1951) Fertilizing capacity of spermatozoa deposited into the fallopian tubes. *Nature*. **168**, 697–698
26. Mariani, N. A. P., Camara, A. C., Silva, A. A. S., Raimundo, T. R. F., Andrade, J. J., Andrade, A. D., Rossini, B. C., Marino, C. L., Kushima, H., Santos, L. D., and Silva, E. J. R. (2020) Epididymal protease inhibitor (EPPIN) is a protein hub for seminal vesicle-secreted protein SVS2 binding in mouse spermatozoa. *Mol. Cell. Endocrinol.* **506**, 110754
27. Silva, E. J. R., Hamil, K. G., Richardson, R. T., and O'Rand, M. G. (2012) Characterization of EPPIN's semenogelin I binding site: a contraceptive drug target. *Biol. Reprod.* **87**, 56
28. Wang, Z., Widgren, E. E., Sivashanmugam, P., O'Rand, M. G., and Richardson, R. T. (2005) Association of eppin with semenogelin on human spermatozoa. *Biol. Reprod.* **72**, 1064–1070
29. Wang, Z., Widgren, E. E., Richardson, R. T., and O'Rand, M. G. (2007) Characterization of an Eppin protein complex from human semen and spermatozoa. *Biol. Reprod.* **77**, 476–484
30. Mitra, A., Richardson, R. T., and O'Rand, M. G. (2010) Analysis of recombinant human semenogelin as an inhibitor of human sperm motility. *Biol. Reprod.* **82**, 489–496
31. Kawano, N., and Yoshida, M. (2007) Semen-coagulating protein, SVS2, in mouse seminal plasma controls sperm fertility. *Biol. Reprod.* **76**, 353–361
32. Araki, N., Kawano, N., Kang, W., Miyado, K., Yoshida, K., and Yoshida, M. (2016) Seminal vesicle proteins SVS3 and SVS4 facilitate SVS2 effect on sperm capacitation. *Reproduction*. 10.1530/REP-15-0551
33. Sakaguchi, D., Miyado, K., Iwamoto, T., Okada, H., Yoshida, K., Kang, W., Suzuki, M., Yoshida, M., and Kawano, N. (2020) Human semenogelin 1 promotes sperm survival in the mouse female reproductive tract. *Int. J. Mol. Sci.* **21**, 3961
34. O'Rand, M. G., Widgren, E. E., Beyler, S., and Richardson, R. T. (2009) Inhibition of human sperm motility by contraceptive anti-eppin antibodies from infertile male monkeys: effect on cyclic adenosine monophosphate. *Biol. Reprod.* **80**, 279–285
35. Silva, A. A. S., Raimundo, T. R. F., Mariani, N. A. P., Kushima, H., Avellar, M. C. W., Buffone, M. G., Paula-Lopes, F. F., Moura, M. T., and Silva, E. J. R. (2021) Dissecting EPPIN protease inhibitor domains in sperm motility and fertilizing ability: repercussions for male contraceptive development. *Mol. Hum. Reprod.* **27**, gaab066
36. O'Rand, M. G., Hamil, K. G., Adevai, T., and Zelinski, M. (2018) Inhibition of sperm motility in male macaques with EP055, a potential non-hormonal male contraceptive. *PloS One*. **13**, e0195953
37. Robert, M., and Gagnon, C. (1999) Semenogelin I: a coagulum forming, multifunctional seminal vesicle protein. *Cell. Mol. Life Sci. CMLS*. **55**, 944–960

38. Kawano, N., Araki, N., Yoshida, K., Hibino, T., Ohnami, N., Makino, M., Kanai, S., Hasuwa, H., Yoshida, M., Miyado, K., and Umezawa, A. (2014) Seminal vesicle protein SVS2 is required for sperm survival in the uterus. *Proc. Natl. Acad. Sci. U. S. A.* **111**, 4145–4150
39. O'Rand, M. G., and Widgren, E. E. (2012) Loss of calcium in human spermatozoa via EPPIN, the semenogelin receptor. *Biol. Reprod.* **86**, 55
40. Katz, D. F., and Vanagimachi, R. (1980) Movement characteristics of hamster spermatozoa within the oviduct. *Biol. Reprod.* **22**, 759–764
41. Silva, E. J. R., Hamil, K. G., and O'Rand, M. G. (2013) Interacting Proteins on Human Spermatozoa: Adaptive Evolution of the Binding of Semenogelin I to EPPIN. *PLoS ONE*. **8**, e82014
42. Kirichok, Y., Navarro, B., and Clapham, D. E. (2006) Whole-cell patch-clamp measurements of spermatozoa reveal an alkaline-activated Ca2+ channel. *Nature*. **439**, 737–740
43. Ren, D., Navarro, B., Perez, G., Jackson, A. C., Hsu, S., Shi, Q., Tilly, J. L., and Clapham, D. E. (2001) A sperm ion channel required for sperm motility and male fertility. *Nature*. **413**, 603–609
44. Young, S., Schiffer, C., Wagner, A., Patz, J., Potapenko, A., Herrmann, L., Nordhoff, V., Pock, T., Krallmann, C., Stallmeyer, B., Röpke, A., Kierzek, M., Biagioni, C., Wang, T., Haalck, L., Deuster, D., Hansen, J. N., Wachten, D., Risse, B., Behre, H. M., Schlatt, S., Kliesch, S., Tüttelmann, F., Brenker, C., and Strünker, T. (2024) Human fertilization in vivo and in vitro requires the CatSper channel to initiate sperm hyperactivation. *J. Clin. Invest.* **134**, e173564
45. Lishko, P., Clapham, D. E., Navarro, B., and Kirichok, Y. (2013) Sperm patch-clamp. *Methods Enzymol.* **525**, 59–83
46. Liu, B., Mundt, N., Miller, M., Clapham, D. E., Kirichok, Y., and Lishko, P. V. (2021) Recording electrical currents across the plasma membrane of mammalian sperm cells. *J. Vis. Exp. JoVE*. 10.3791/62049
47. Mannowetz, N., Naidoo, N. M., Choo, S.-A. S., Smith, J. F., and Lishko, P. V. (2013) Slo1 is the principal potassium channel of human spermatozoa. *eLife*. **2**, e01009
48. de Lamirande, E., and Lamothe, G. (2010) Levels of semenogelin in human spermatozoa decrease during capacitation: involvement of reactive oxygen species and zinc. *Hum. Reprod. Oxf. Engl.* **25**, 1619–1630
49. Araki, N., Trencsényi, G., Krasznai, Z. T., Nizsalóczki, E., Sakamoto, A., Kawano, N., Miyado, K., Yoshida, K., and Yoshida, M. (2015) Seminal vesicle secretion 2 acts as a protectant of sperm sterols and prevents ectopic sperm capacitation in mice. *Biol. Reprod.* **92**, 8
50. Wang, D., Hu, J., Bobulescu, I. A., Quill, T. A., McLeroy, P., Moe, O. W., and Garbers, D. L. (2007) A sperm-specific Na+/H+ exchanger (sNHE) is critical for expression and in vivo bicarbonate regulation of the soluble adenylyl cyclase (sAC). *Proc. Natl. Acad. Sci. U. S. A.* **104**, 9325–9330
51. Novero, A. G., Torres Rodríguez, P., De la Vega Beltrán, J. L., Schiavi-Ehrenhaus, L. J., Luque, G. M., Carruba, M., Stival, C., Gentile, I., Ritagliati, C., Santi, C. M., Nishigaki, T., Krapf, D., Buffone, M. G., Darszon, A., Treviño, C. L., and Krapf, D. (2024) The sodium-proton exchangers sNHE and NHE1 control plasma membrane hyperpolarization in mouse sperm. *J. Biol. Chem.* **300**, 107932
52. Wang, H., McGoldrick, L. L., and Chung, J.-J. (2021) Sperm ion channels and transporters in male fertility and infertility. *Nat. Rev. Urol.* **18**, 46–66
53. Chávez, J. C., Ferreira, J. J., Butler, A., De La Vega Beltrán, J. L., Treviño, C. L., Darszon, A., Salkoff, L., and Santi, C. M. (2014) SLO3 K+ channels control calcium entry through CATSPER channels in sperm. *J. Biol. Chem.* **289**, 32266–32275
54. Navarro, B., Kirichok, Y., and Clapham, D. E. (2007) KSper, a pH-sensitive K+ current that controls sperm membrane potential. *Proc. Natl. Acad. Sci. U. S. A.* **104**, 7688–7692
55. Kawano, N., Yoshida, K., Iwamoto, T., and Yoshida, M. (2008) Ganglioside GM1 mediates decapacitation effects of SVS2 on murine spermatozoa. *Biol. Reprod.* **79**, 1153–1159